Dalton Transactions

ROYAL SOCIETY OF CHEMISTRY

PAPER

View Article Online
View Journal | View Issue

Check for updates

Cite this: *Dalton Trans.*, 2025, **54**, 5391

Published on 26 February 2025. Downloaded on 4/3/2026 1:25:21 AM.

Tailoring the local environment of Ln^{3+} in pyridine-based complexes: effect on the thermodynamic, kinetic, structural and relaxation properties†

Martina Sanadar, [a] Loëza Collobert,[a] Harlei Martin, [a] Jean-François Morfin,[a] Zoltán Garda, [a,d] Agnès Pallier,[a] Serge Gambarelli,[b] Andrea Melchior[c] and Célia S. Bonnet *[a]

Received 29th January 2025,
Accepted 25th February 2025

DOI: 10.1039/d5dt00236b

rsc.li/dalton

The replacement of one or two negatively charged carboxylate functions by neutral pyridine or imidazole pendant groups in pyridine-based polyaminopolycarboxylate ligands was investigated. Four ligands were synthesized and the thermodynamic, kinetic, structural and relaxation properties of their corresponding Ln^{3+} complexes was thoroughly studied. The protonation constants of the ligands as well as the stability constants of the corresponding Ln^{3+} complexes were determined by pH potentiometric measurements. While no strong effect on the stability constants of the Ln^{3+} complexes is observed when one carboxylate is replaced by an imidazole or a pyridine, the replacement of two carboxylate functions is detrimental to the overall stability of the complexes. The dissociation kinetics of GdImPy and GdPyPy, evaluated through Eu^{3+}-exchange reactions, predominantly proceed *via* an acid-catalyzed mechanism, with minimal direct Eu^{3+} attack. The presence of a protonatable function on the imidazole ring leads to more labile complexes. NMR and luminescence studies combined with DFT calculations evidenced the coordination of the imidazole or pyridine pendant arms. The Gd^{3+} complexes exhibit high relaxivity values (r_1 = 8.25 mM^{-1} s^{-1} and 7.97 mM^{-1} s^{-1} at 60 MHz and 25 °C for GdImPy and GdPyPy, respectively) in accordance with their bishydrated character, and no aggregation phenomena are observed over a wide range of concentrations. Variable-temperature ^{17}O NMR and NMRD data analysis of GdImPy and GdPyPy provided insights into the microscopic parameters affecting their relaxation properties. Interestingly, the water exchange rate is strongly accelerated with the imidazole pendant arm compared to the pyridine, which could be related to steric crowding around the Ln^{3+} ion. The two inner-sphere water molecules are not displaced by interactions with biological anions such as citrate and phosphate. However, a relaxivity decrease of *ca.* 30% is observed in the presence of carbonate, as confirmed by ^{1}H relaxivity and luminescence lifetime measurements.

Introduction

Lanthanide (Ln) compounds have been extensively used in the last decades in medicine, telecommunications, material chemistry, lasers, and biosciences.[1] Their popularity in medicine is certainly due to the extensive use of Gd^{3+} chelates as contrast agents in magnetic resonance imaging (MRI). Given the fact that they are non-endogenous, and they have a similar radius to Ca^{2+}, Ln^{3+} ions are toxic and must be encapsulated within complexes that are both thermodynamically stable and kinetically inert.[2,3] The effectiveness of these contrast agents, often measured by proton relaxivity (r_1), is influenced by several factors including the number of water molecules directly coordinated to the Gd^{3+} ion, their exchange rate with bulk water, the rotational correlation time of the complex, and its electronic relaxation, all of which are tied to the complex's structural characteristics. Understanding these structure-efficacy relationships is essential for designing more effective contrast agents. For enhanced stability in complexation and improved contrast efficiency, developments have focused on designing

[a]*Centre de Biophysique Moléculaire, CNRS UPR 4301, Université d'Orléans, rue Charles Sadron, 45071 Orléans, France. E-mail: celia.bonnet@cnrs.fr*
[b]*University Grenoble Alpes, CEA, CNRS, IRIG, SyMMES, CAMPE, F-38000 Grenoble, France*
[c]*Polytechnic Department, University of Udine, Chemical Technologies Laboratories, via del Cotonificio 108, 33100 Udine, Italy*
[d]*Department of Physical Chemistry, University of Debrecen, Egyetem tér 1, 4010 Debrecen, Hungary*

† Electronic supplementary information (ESI) available. See DOI: https://doi.org/10.1039/d5dt00236b

Published on 26 February 2025. Downloaded on 4/3/2026 1:25:21 AM.

heptadentate and octadentate ligands, optimized to accommodate the high coordination demands of Ln^{3+} ions.[3] Typically, acyclic ligands such as DTPA (diethylenetriaminepentaacetic acid) and its derivatives, or macrocyclic ligands like DOTA (1,4,7,10-tetraazacyclododecane-1,4,7,10-tetraacetic acid) and its derivatives are commonly used as Ln^{3+} chelators.[4,5] Both ligand types coordinate Gd^{3+} in an octadentate fashion, forming kinetically inert and thermodynamically stable complexes with one water molecule in the first coordination sphere. Significant efforts have been made to modify these parent complexes, GdDOTA and GdDTPA, to enhance their relaxation properties.[6] Recently, the first bishydrated contrast agent was clinically approved,[7] paving the way for the development of contrast agents with higher relaxivity without compromising thermodynamic stability or kinetic inertness.

In this regard, we have been interested in pyridine-based polyaminocarboxylate ligands (Py, Fig. 1), which form bishydrated Ln^{3+} complexes. These ligands offer a flexible platform for designing contrast agents with optimized properties as the two water molecules are not replaced by physiological cations,[8] and the complexes show no acute or long-term toxicity.[9] While possessing a bishydrated character, they were demonstrated to be efficient bimodal contrast agents suitable for both MRI (using Gd^{3+} complexes) and near-infrared (NIR) optical imaging (using Nd^{3+} and Yb^{3+} complexes). The latter properties can be optimized by incorporating triazole or isoquinoline moieties into the pyridine structure.[9,10] The addition of a Zn^{2+} complexing unit has enabled Zn^{2+} sensing,[11] as well as Zn^{2+} quantification using $^{165}Er^{3+}$.[12] Further modifications enabled the elucidation and rationalization of their Zn^{2+} response, as well as their *in vivo* application.[12–14] From a more fundamental point of view, we explored the effect of structural modifications, such as the introduction of methyl hydrazine groups (HYD, Fig. 1), on the coordination properties.[15] Similarly, the introduction of a triazine scaffold was also explored (PTDITA, Fig. 1) by Botta and co-workers.[16]

Building on this approach, and to expand the family of such versatile compounds, we have designed four ligands (see Fig. 2) where one or two carboxylate functions have been replaced by pyridine or imidazole groups. In this work, we report the synthesis of Im2Py and Py3, as well as a detailed thermodynamic, kinetic, and structural study of the four Ln^{3+} complexes (Fig. 2), using potentiometry, EPR, NMR, UV-visible and luminescence spectroscopy, as well as DFT calculations. The microscopic parameters influencing the relaxivity of the Gd^{3+} complexes have been determined by ^{1}H relaxometry and

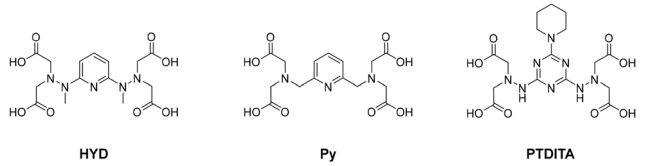

Fig. 1 Chemical structure of pyridine-based polyaminopolycarboxylate ligands previously reported in the literature.

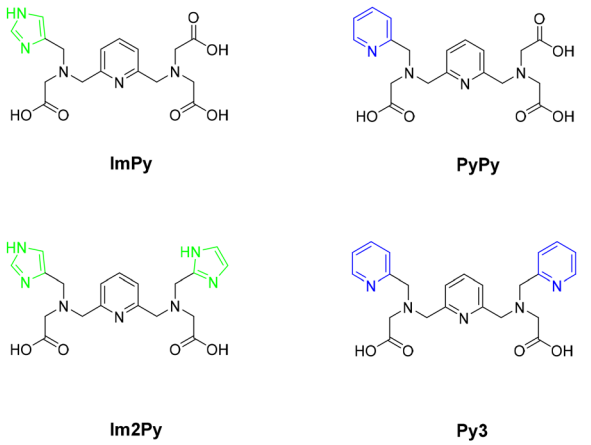

Fig. 2 Chemical structure of the ligands discussed in this work.

^{17}O NMR, and the effect of endogenous anions has also been studied in detail.

Recent studies have highlighted the effect of the replacement of a carboxylate function on DOTA-type ligands by a substituted pyridine[17] or an imidazothiadiazole[18] on the thermodynamic stability, kinetic inertness and water exchange rate of the complexes. To the best of our knowledge, no such comprehensive studies have been conducted on imidazole moieties, and importantly the systematic comparison of a negatively charged carboxylate function with a 6-membered ring pyridine or a 5-membered ring imidazole on the characteristic of the Ln^{3+} complexes has never been performed. This should give important insights into the design of multimodal or responsive contrast agents in the future.

Results and discussion

Synthesis of ligands

The synthesis of ImPy and PyPy is described elsewhere.[19] The synthesis of ligands Im2Py and Py3 was achieved in 4 steps starting from commercially available 1-trityl-1*H*-imidazole-4-carbaldehyde or 2-picolylamine (see Fig. 3 and ESI†). The first step involved the formation of an intermediate containing an ester and the heterocycle imidazole or pyridine through a reductive amination for Im2Py (compound 1) or a mono-*N*-alkylation for Py3 (compound 4). This intermediate block was then attached to the commercially available 2,6-bis(bromomethyl)pyridine (compound 2 and 5). Finally, the desired ligands were obtained after the removal of the protecting groups.

Protonation constants of ligands and stability constants of the complexes

Potentiometric studies were performed on ImPy, Im2Py, PyPy and Py3, to determine the species present in solution through the evaluation of their equilibrium constants (Fig. 4 and S1–4†).

This journal is © The Royal Society of Chemistry 2025

Published on 26 February 2025. Downloaded on 4/3/2026 1:25:21 AM.

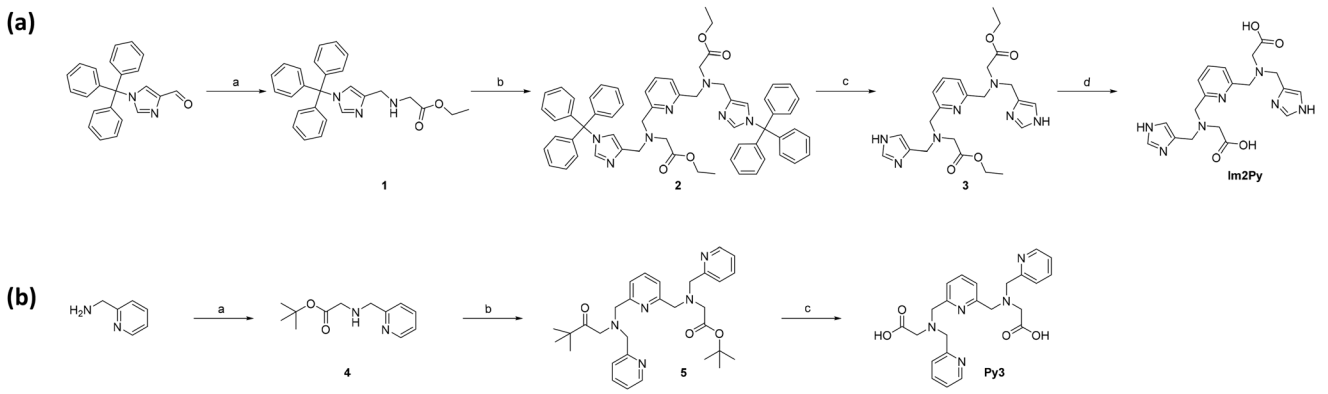

Fig. 3 (a) Synthesis of the ligand Im2Py. Reagents and conditions: (a) ethyl glycinate hydrochloride, NEt_3, acetic acid, DCM, $NaBH(OAc)_3$, rt, 24 h; (b) 2,6-bis(bromomethyl)pyridine, K_2CO_3, ACN, reflux, 12 h; (c) TFA, DCM, 4 h, rt; (d) LiOH, THF : H_2O (1 : 1 v/v), 12 h, rt. (b) Synthesis of the ligand Py3. Reagents and conditions: (a) *tert*-butyl bromoacetate, K_2CO_3, ACN, reflux, 4 h; (b) 2,6-bis(bromomethyl)pyridine, K_2CO_3, ACN, reflux, 18 h; (c) 1,4-dioxane, HCl, 2 h, rt.

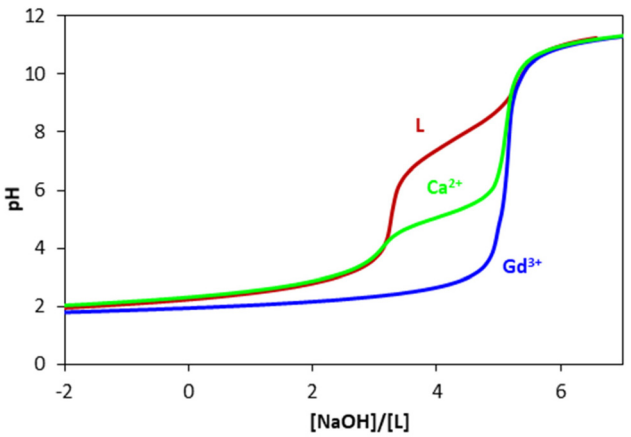

Fig. 4 Potentiometric titration curves of PyPy (2.83 mM) in the absence and in the presence of 1 eq. of Ca^{2+} and Gd^{3+} in NaCl 0.1 M at 25 °C.

The ligand protonation constants were assessed, as defined in eqn (1):

$$K_i = \frac{[H_iL]}{[H_{i-1}L][H]} \quad (1)$$

The ligands ImPy/Im2Py and PyPy/Py3 have 4 and 5 protonation constants, respectively (Table 1). For comparison, Py has 4 protonation constants, with the two highest corresponding to the tertiary amines and the two lowest to carboxylate functions.[8] The protonation of the other carboxylate functions and the central pyridine is too low to be observed. The first two protonation constants of ImPy/Im2Py/PyPy/Py3 correspond to the protonation of the tertiary amines. Notably, replacing a carboxylate group with an imidazole or a pyridine reduces the protonation constants of these amines, with a more pronounced effect in the case of the pyridine. Indeed, imidazole or pyridine are more electron-withdrawing than a carboxylate function, making the proton of the tertiary amine more acidic. For ImPy and Im2Py, the third protonation constant, approximately 4.5, is higher than that of PyPy and Py3 and corresponds to the protonation of the imidazole function. ^{1}H NMR titrations of ImPy were conducted in the pD range 1.93–11.95 to support this hypothesis (Fig. S6†). Indeed, an important shift of the H of the imidazole ring is observed in this pD range. The titration data were fitted with HypNMR,[20] resulting in a protonation constant of 4.61(4), consistent with $\log K_{H3}$ determined by pH-potentiometric titrations. This is also in agreement with literature data, which report a protonation constant of 4.73 for 4-aminomethylimidazole.[21] The final protonation constant of ImPy corresponds to the protonation of a carboxylate function, while for Im2Py, it could be either a carboxylate function or the second imidazole group.

Table 1 Protonation constants measured in NaCl 0.1 M at 25 °C

$\log K_H$	ImPy	Im2Py	PyPy	Py3	HYD[a 15]	Py[a 8]	PTDITA[a 16]
$\log K_{H1}$	8.6(1)	8.34(8)	8.35(5)	7.37(5)	9.30	8.95	8.05
$\log K_{H2}$	7.84(4)	7.0(1)	7.10(2)	6.55(7)	4.95	7.85	4.71
$\log K_{H3}$	4.46(8)	4.52(9)	2.95(6)	3.15(9)	4.26	3.38	4.02
$\log K_{H4}$	2.09(4)	3.2(1)	1.98(8)	2.69(4)	3.94	2.48	3.36
$\log K_{H5}$	—	—	1.7(1)	1.6(1)	3.29	—	3.00
$\log K_{H6}$	—	—	—	—	2.60	—	1.92
$\sum \log K_{Hi}$	22.99	23.06	22.08	21.36	28.34	22.66	25.06

[a] I = 0.1 M KCl and 25 °C.

Published on 26 February 2025. Downloaded on 4/3/2026 1:25:21 AM.

Regarding PyPy and Py3, three protonation constants are observed between 3 and 1.6, likely corresponding to the protonation of carboxylate functions and/or the nitrogen of the pendant pyridine arm. Indeed, the protonation constant of the tertiary nitrogen of 2-methylpyridine is reported to be 2.28 in the literature.[22] Finally, it is clear that the overall basicity of the ligands containing imidazole groups is higher.

Complex stability and protonation constants, $\log K_{ML}$, $\log K_{MLH}$ and $\log K_{MLOH}$ (eqn (2)–(4)) have been determined for Gd^{3+} (Fig. 4, S1–S4† and Table 2).

$$K_{ML} = \frac{[ML]}{[L][M]} \quad (2)$$

$$K_{MLH_i} = \frac{[ML]}{[MLH_{i-1}][H]} \quad (3)$$

$$K_{MLOH} = \frac{[ML]}{[ML(OH)][H]} \quad (4)$$

The different species formed and their stability constants are summarised in Table 2. The formation of Gd^{3+} complexes is observed (Fig. S7–10†), along with a protonation constant in the case of ImPy and Im2Py.

Additionally, in some cases, a soluble monohydroxocomplex forms at high pH levels. The replacement of carboxylate functions by pyridine or imidazole is expected to decrease the stability of the corresponding Ln^{3+} complexes, as a negatively charged function is replaced by an aromatic nitrogen atom. The effect is limited with the monosubsituted ligands, as the stability constants of Gd^{3+} complexes formed with ImPy and PyPy are one to two orders of magnitude lower than those of GdHYD, GdPy and GdPTDITA. However, for the bisubstituted ligands Py3 and Im2Py, the Gd^{3+} stability constants are five orders of magnitude lower than that of GdPy. Recently, an empirical formula to predict the stability constants of Gd^{3+} complexes with the most common donor atoms was developed.[5] The experimental stability constants found here agree well with the calculated values ($\log K_{calc}$ = 19.22, 16.84, 14.46 for GdPy, GdPyPy, and GdPy3 respectively). The relatively more important decrease in stability constants when a second carboxylate is substituted by a pyridine could be explained by entropic and enthalpic effects. When GdPyPy is formed, the resulting species is neutral, thus exerting a less important ordering effect towards the outer sphere solvent with respect to the positively charged GdPy3 complex. Secondly, the addition of pyridine groups causes an increased steric hindrance in the complex and modified electrostatic repulsion between the carboxylate functions. The latter effect was evidenced by DFT calculations (*vide infra*, and Fig. S15 and Table S1†). All together, these stability constants result in pGd values of approximately 16–17 for the monosubstituted ImPy and PyPy complexes, and around 13 for the disubstituted Im2Py and Py3 complexes. Interestingly, the loss in stability is higher with the imidazole compared to the pyridine group, as can be deduced from the pGd values. A protonated complex is present in the case of GdImPy and GdIm2Py, likely due to the protonation of the imidazole. The speciation was confirmed by both r_1 measurements as a function of pH, and ^{1}H NMR titrations on the corresponding diamagnetic Y^{3+} complexes (*vide infra*).

To evaluate the selectivity of ImPy/Im2Py/PyPy/Py3 for Gd^{3+} over other key physiological cations, potentiometric titrations were conducted with Zn^{2+}, Cu^{2+} and Ca^{2+}. Indeed, transmetallation with endogenous cations lead to the release of toxic Ln^{3+} ions. The stability constants of ZnImPy and ZnPyPy have been described elsewhere.[19] While, the replacement of carboxylate functions by one or two pyridine groups, or one imidazole group has no effect on the stability of the complexes, the substitution of a second carboxylate function by an imidazole group dramatically decreases the Zn^{2+} stability constant by four orders of magnitude. A protonation constant is observed for all the complexes, around 3.5 for ZnPy3 and ZnPyPy, and around 5.2 for ZnImPy and ZnIm2Py. These high values suggest that the protonation constant probably occur on an aliphatic nitrogen. In the case of ZnIm2Py, two protonation constants are observed.

Regarding the calcium stability constants, they are one order of magnitude lower than that of CaPy when one carboxylate function is replaced by a pyridine or an imidazole, and three orders of magnitude lower when two carboxylate functions are replaced. Except for CaPy3, all the complexes have one protonation constant.

Table 2 Stability constants of the different complexes measured in NaCl 0.1 M at 25 °C

log *K*	ImPy	Im2Py	PyPy	Py3	HYD[15]	Py[8]	PTDITA[16]
GdL	17.02(4)	13.64(3)	16.87(9)	13.35(6)	18.33	18.60	18.49
GdLH	3.19(6)	3.47(4)	—	—	3.06	—	2.81
GdLOH	11.13(3)	—	11.2(1)	11.01(5)	11.0	—	10.43
pGd[a]	16.21	13.49	16.68	13.95	17.4	17.4	18.6
ZnL	15.2[b]	11.1(1)	15.33[b]	15.03(7)	16.27	15.84	15.33
ZnLH	5.11[b]	5.21(7)	3.52[b]	3.53(8)	4.03	3.81	3.69
$ZnLH_2$	—	2.32(7)	—	—	3.0	—	2.15
ZnLOH	10.68[b]	—	—	—	11.08	—	10.61
CaL	7.80(1)	6.17(6)	8.19(5)	6.29(2)	9.21	9.43	9.79
CaLH	6.7(1)	6.6(1)	4.81(4)	—	3.85	—	3.86

[a] $pGd = -(\log[Gd^{3+}]_{free})$ at pH 7.4 with $[Gd^{3+}]$ = 1 μM and [L] = 10 μM. [b] Ref. 19.

 This journal is © The Royal Society of Chemistry 2025

Published on 26 February 2025. Downloaded on 4/3/2026 1:25:21 AM.

Altogether, this means that except for Py3, which presents a particularly high Zn^{2+} stability constant, all the other ligands remain selective for Gd^{3+} *vs.* Ca^{2+} or Zn^{2+}.

The case of Cu^{2+} is more complex, as pH-potentiometric titrations have historically underestimated the stability of these complexes. It has been demonstrated that UV-visible titrations, or a combination of pH-potentiometry and UV-visible spectrophotometry, are essential for obtaining accurate and definitive stability constants.[15,23,24] A key challenge in analysing pH-potentiometric data is that seemingly reasonable species models often provide acceptable fits. For instance, the presence of fully formed protonated complexes at low pH can artificially account for the absence of free Cu^{2+} in the sample. UV-visible spectra were recorded (Fig. S11–13†) and it is clear that the complexes are already formed at high acidic concentrations. Moreover, very clear changes in the maximum of the absorption bands are observed, indicating conformational changes in the complexes. This was also confirmed by EPR measurements at pH *ca.* 2 (Fig. S14†), showing the presence of two species with different hyperfine and *g* values concomitant with different first coordination sphere of Cu^{2+}. This prevented us from determining reliable stability constants.

Kinetic inertness

Kinetic inertness is another crucial factor when evaluating the toxicity of a given complex. Numerous reports have highlighted that kinetic inertness often outweighs the importance of the thermodynamic stability constant. To assess the kinetic inertness of GdImPy and GdPyPy, we follow the dissociation of the complexes using Eu^{3+} as a competitor to accelerate the dissociation process. The dissociation (eqn (5)) was followed between pH 4.7–6.11 for GdImPy, and pH 3.59–5.05 for GdPyPy by monitoring the formation of the EuL complexes by luminescence, with a significant (10 fold) excess of Eu^{3+} to ensure pseudo-first-order conditions.

$$[GdL] + Eu^{3+} \rightleftharpoons [EuL] + Gd^{3+} \quad (5)$$

$$-\frac{d[LnL]_t}{dt} = k_{obs}[LnL]_t \quad (6)$$

The use of higher Eu^{3+} concentrations (40 eq.) did not result in significant differences in the observed k_{obs}, as was the case for the parent GdPy[8] and other complexes of this family.[12] This indicates that both spontaneous and proton-assisted dissociations are the main pathways, as illustrated in Scheme 1.

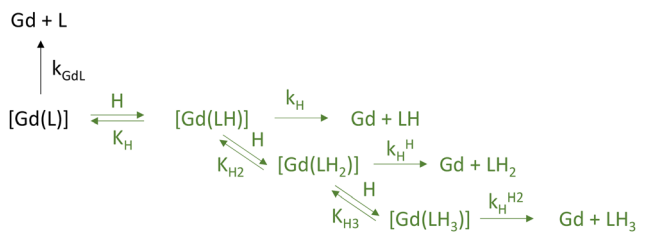

Scheme 1 Reaction mechanism of the dissociation of GdL (charges are omitted for clarity).

The dissociation follows pseudo-first order kinetics (eqn (6)) and the dissociation rate is directly proportional to the total concentration of the complex $[LnL]_t$ (corresponding to the sum of the concentration of protonated and non-protonated complexes), where k_{obs} is the observed pseudo-first order rate constant.

The concentration of GdL can be given as the sum of the concentrations of the different reactive species (eqn (7)):

$$[GdL]_t = [GdL] + [Gd(LH)] + [Gd(LH_2)] \quad (7)$$

Therefore,

$$k_{obs}[GdL]_t = k_{GdL}[GdL] + k_H[Gd(LH)] + k_{H2}[Gd(LH_2)] \quad (8)$$

Considering the complex protonation constants (K_1 = [GdLH]/[GdL][H^+], and K_2 = [$GdLH_2$]/[GdLH][H^+]), k_{obs} can be expressed as follows:

$$k_{obs} = \frac{k_0 + k_1[H^+] + k_2[H^+]^2|}{1 + K_1[H^+] + K_2K_1[H^+]^2} \quad (9)$$

where $k_0 = k_{GdL}$, $k_1 = k_HK_1$, $k_2 = k_{H2}K_1K_2$.

The k_{obs} values increase with increasing H^+ concentration, and the best fit of the data to eqn (9) is illustrated in Fig. 5. In the fitting, the constant characteristic for the spontaneous dissociation, k_0, was always found to be very close to zero or with a small negative value, and a large standard deviation. It was consequently fixed to zero in the fitting process.

The situation is different for GdImPy and GdPyPy, as GdImPy has a protonation constant K_1 of 1550 (±200) as determined by pH-potentiometric titration, which is not the case for GdPyPy. In the case of GdImPy, a second protonation constant K_2 could not be determined as it should be even smaller than K_1, and in the pH-range studied the term $K_2K_1[H^+]_2$ is likely negligible *vs.* 1. For GdPyPy, even the first protonation constant K_1 could not be determined (it could not be obtained by pH-potentiometric titrations) as even the term K_1 [H^+] is likely negligible in this case, similarly to what was observed for

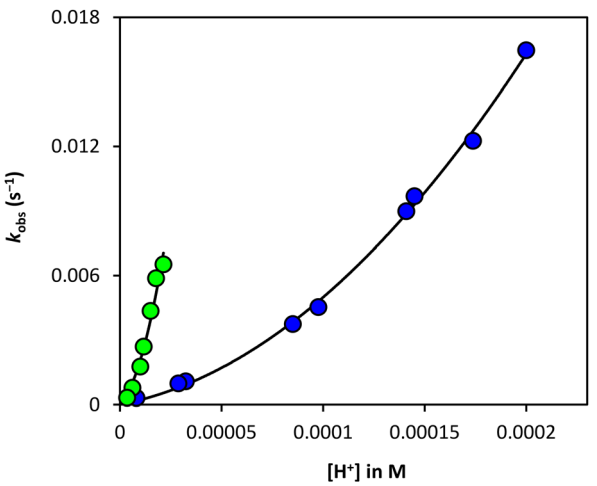

Fig. 5 k_{obs} *versus* H^+ concentration for the reaction of GdImPy (126 μM; ●) and GdPyPy (122 μM, ●) with Eu^{3+} (1.22 mM) at 25 °C, in 0.1 M NaCl. The lines represent the best fit to eqn (9).

Published on 26 February 2025. Downloaded on 4/3/2026 1:25:21 AM.

Table 3 Rate constants characterizing the dissociation of the Gd^{3+} complexes of ImPy, PyPy, Py and DTPA (25 °C)

	GdImPy	GdPyPy	GdPy[12]	GdDTPA[25]
k_1 (M^{-1} s^{-1})	93 ± 10	18.4 ± 0.8	3.7	0.58
k_2 (M^{-2} s^{-1})	(1.16 ± 0.06) × 10^7	(3.15 ± 0.05) × 10^5	3.1 × 10^4	9.7 × 10^4
K^{H}	1549[a]	—	—	100[a]
$t_{1/2}$ (pH 7.4/h)	51.7	263	1307	202

[a] Determined by pH-potentiometric titrations.

GdPy. It should be noted that even in the case of GdImPy, for which K_1 was fixed to the potentiometric value, the term $K_1[H^+]$ is smaller than 1 in the pH-range studied.

The results of the fitting are presented in Table 3. Both k_1 and k_2 are higher in the case of GdImPy and GdPyPy *vs.* GdPy. DFT calculations (*vide infra*) show that the Eu–$N_{Im/Py'}$ distance in EuPyPy is longer (*ca.* 0.2 Å) compared to that of Eu–O_{COO} in EuPy evidencing a less constrained environment around the Ln^{3+}, which could explain the lower kinetic inertness for these complexes. Finally, the kinetic constants characterizing GdPyPy are one to two orders of magnitude higher compared to those characterizing GdImPy. This can be explained by the presence of the protonation site of the imidazole, close to the metal ion, that accelerates the proton assisted dissociation. The half-lives extrapolated at pH 7.4, show values five and 25 times lower for GdPyPy, and GdImPy with respect to GdPy, respectively. The value for GdPyPy is in the same range as that of GdDTPA, as the formation of binuclear species, absent here, is the driving force of dissociation in the latter case.

Structure of the Ln^{3+} complexes

The coordination sphere of Ln^{3+} complexes (number of water molecules directly coordinated, rigidity of the complex, Ln-ligand distances) will significantly impact their thermodynamic stability, kinetic inertness and relaxation properties. To gain insight into the structural modifications resulting from the replacement of a carboxylate function by a pyridine or an imidazole, we performed experimental ^1H and 2D $^1H/^{13}C$ NMR spectra on the corresponding diamagnetic Y^{3+} complexes, luminescence spectroscopy on the Eu^{3+} complexes, as well as DFT calculations.

First, ^1H NMR titrations have been performed as a function of pH (Fig. S16 and S17†). For YImPy, at very low pD (below 2.44), the spectra primarily show the protonated ligand. Between pD 3.14 and 4.99, the spectra are very broad, with a quasi-disappearance of the proton of the imidazole ring. From pD 5.77 and above, well defined spectra showing the presence of a single species are observed (Fig. S16a and S16b†). This aligns well with the species distribution obtained by potentiometry (Fig. S7†). It confirms that the protonation of the complex occurs on the imidazole ring and indicates that YImPyH is a highly flexible system, which is not the case for YImPy. The case of PyPy is simpler. From pD of 2.72 no change in the spectra occurred (Fig. S17a and S17b†), consistent with the absence of protonated species.

f–f transitions are forbidden, therefore direct excitation of Ln^{3+} complexes are not very efficient, and the excitation is often performed through a chromophore that transfers its energy to the excited state of the Ln^{3+}, which is called the "antenna effect".[26–28] Luminescence spectra can give complementary information on the structure of the complexes. It has been previously shown that the pyridine chromophore in this family of complexes can sensitize the luminescence of Eu^{3+}.[8,29,30] The normalized luminescence spectra at physiological pH, obtained following excitation at the absorption maxima for the EuImPy/EuIm2Py/EuPyPy/EuPy3 complexes, as well as EuPy, are presented in Fig. S18.† The replacement of carboxylate functions by pyridine or imidazole groups yields ligands that can still sensitize Eu^{3+} luminescence, and typical Eu^{3+} spectra are observed. Quantum yields were not measured, so it is not possible to determine from these spectra how Eu^{3+} luminescence sensitization is affected; however, some conclusions can still be drawn by comparing these spectra. In particular, the ΔJ = 2 and 4 transitions, centred around 616 and 690 nm respectively, are sensitive to the environment, whereas this is less true for the ΔJ = 1 transition (centered around 592 nm). From Fig. S18,† it is clear that the addition of two pyridines or two imidazoles (EuPy3 and EuIm2Py) has a strong impact on the shape and intensity of the bands at 616 nm and 690 nm, respectively. The intensity ratio of the $\Delta J = 2/\Delta J = 1$ bands are 2.34, 2.32, 2.58, 3.00, and 1.59 for EuPy, EuImPy, EuPyPy, EuIm2Py, and EuPy3, respectively. This clearly indicates different environments for EuIm2Py and EuPy3 compared to the reference compound EuPy.

The number of water molecules in the first coordination sphere of the metal ion can be determined using an empirical formula based on the lifetime measurements of the complexes in light water (H_2O) and heavy water (D_2O) when the deactivation of Ln^{3+} is primarily due to vibrational oscillations of O–H, C–H, or N–H bonds.[31] The empirical formula used in our case is as follows:

$$q = 1.11(\tau_{H_2O}{}^{-1} - \tau_{D_2O}{}^{-1} - 0.31) \quad (10)$$

where τ represents the luminescence lifetimes in ms.

To determine the lifetimes, the intensity of the emission band of the complex at 616 nm was monitored over time after excitation at the appropriate wavelength for each complex. All data could be fitted with mono-exponential decay functions, indicating that only one species is present in solution at pH 7.4, in accordance with NMR data. The results are presented in Table 4.

For comparison, the luminescence lifetimes of EuPy were also measured in the same conditions, and they are all similar. All the complexes have two water molecules in the first coordi-

 This journal is © The Royal Society of Chemistry 2025

Published on 26 February 2025. Downloaded on 4/3/2026 1:25:21 AM.

Table 4 Luminescence lifetimes of Eu^{3+} complexes (λ_{em} = 616 nm) in H_2O and D_2O (pH/pD = 7.4; [ImPy] = 82.95 μmol, λ_{exc} = 262 nm; [Im2Py] = 105.10 μmol, λ_{exc} = 263 nm; [PyPy] = 93.49 μmol, λ_{exc} = 261 nm; [Py3] = 83.01 μmol, λ_{exc} = 262 nm)

	τ_{H_2O}	τ_{D_2O}	q
ImPy	0.390(5)	2.24(1)	2.0(2)
Im2Py	0.398(5)	2.16(1)	1.9(2)
PyPy	0.406(8)	2.06(1)	1.9(2)
Py3	0.414(3)	1.90(1)	1.8(2)
Py	0.395(5)	2.30(1)	2.0(2)

nation sphere of Eu^{3+}. This most likely means that the nitrogen atoms of the pyridine or imidazole groups coordinate Eu^{3+}, resulting in heptadentate ligands (4 N and 3 O or 5 N and 2 O in the coordination sphere of Eu^{3+} for ImPy/PyPy and Im2Py/Py3, respectively).

This was further confirmed by NMR experiments (Fig. 6 and S19†). A full attribution of the NMR spectra of YImPy and YPyPy was performed (Table S2†) using 2D $^1H/^{13}C$ HSQC and HMBC experiments. The spectra provide evidence for the formation of a single isomer for YImPy, while for YPyPy a minor isomer (*ca.* 10–15%) can also be evidenced. For the major species, the presence of non-equivalent protons on the imidazole or pyridine arms (H_{14}, Fig. 6) of YImPy and YPyPy, respectively, confirms the coordination of the imidazole and the pendant pyridine to Y^{3+}.

Finally, DFT calculations are in agreement with a coordination model with 2 coordinated water molecules (Fig. 7), where the Eu^{3+} ion is 9-coordinated. The calculated bond distances for the tertiary amine nitrogen atoms in ImPy and PyPy and acetate oxygens (Table 5) are in the range found in the solid state of other polyaminopolycarboxylate complexes.[32] Clearly the replacement of a carboxylate function by an imidazole or a pyridine group results in longer Eu–$N_{Py'/Im}$ distances than that of Eu–O_{COO}, with increased length of 0.17 Å and 0.24 Å for EuImPy and EuPyPy, respectively. These differences are consistent both with the lower thermodynamic stability

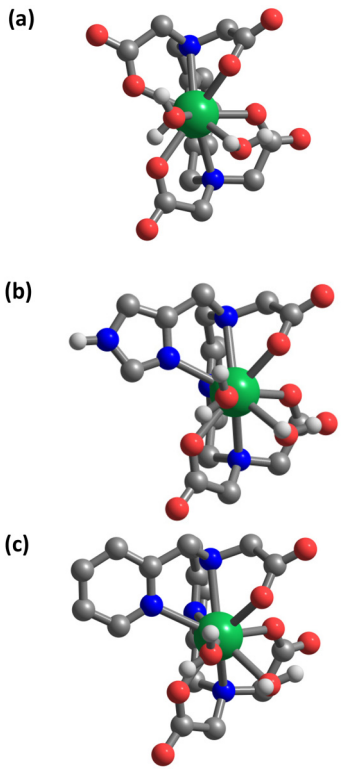

Fig. 7 Lowest energy structures of the $[Eu(L)(H_2O)_2]^-$ complex species. L = Py (a), ImPy (b), PyPy (c). Hydrogen atoms bound to carbons are hidden for clarity.

and kinetic inertness of the Ln^{3+} complexes with ImPy and PyPy with respect to Py. Interestingly, the Eu–$N_{Py'}$ distance in EuPyPy is 0.07 Å longer than that of Eu–N_{Im} in EuImPy. Finally, small differences in the Eu–O_w are observed for the three complexes.

Relaxation properties

To characterize the parameters influencing proton r_1 in GdImPy and GdPyPy, nuclear magnetic relaxation dispersion

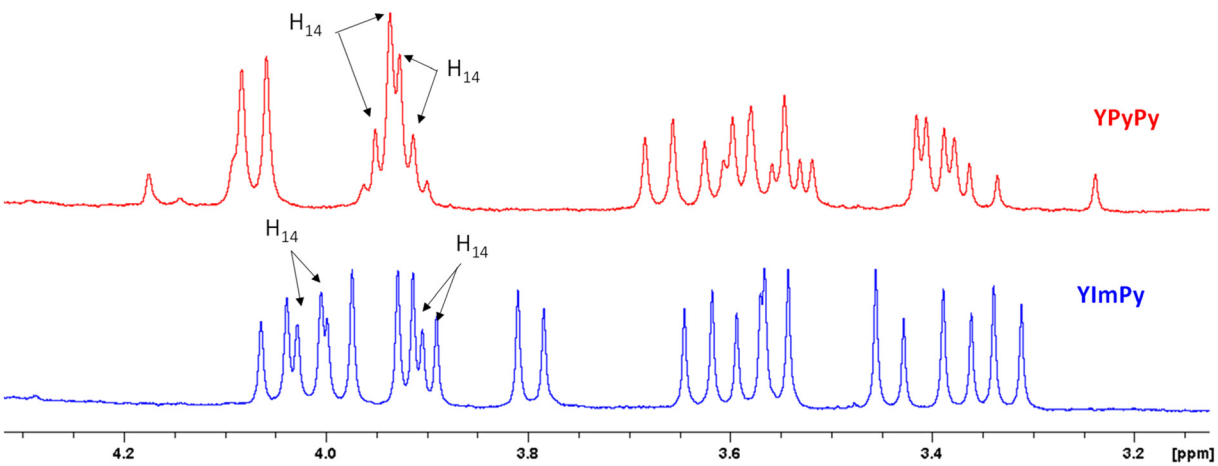

Fig. 6 ^1H NMR spectra of YPyPy and YImPy (aliphatic part) at pD 7.4.

Published on 26 February 2025. Downloaded on 4/3/2026 1:25:21 AM.

Table 5 Relevant bond distances (Å) of the minimum-energy structures of selected Eu^{3+} complexes. N_{py}: nitrogen of the pyridine core. N_{am}: nitrogen of the tertiary amines. $N_{im/py'}$: nitrogen of the pendant heterocycle. O_{COO}: oxygen of acetate group(s). O_W: oxygen of water molecules. For Eu–O_{COO} bonds, the average value is reported

	$[EuPy(H_2O)_2]^-$	$[EuImPy(H_2O)_2]$	$[EuPyPy(H_2O)_2]$
Eu–N_{py}	2.633	2.628	2.626
Eu–O_{COO}	2.41	2.40	2.39
Eu–N_{am}	2.676, 2.705	2.678, 2.714	2.682, 2.684
Eu–$N_{im/Py'}$	—	2.572	2.643
Eu–O_W	2.571, 2.616	2.553, 2.607	2.553, 2.570

(NMRD) profiles were recorded over a field range of 10 kHz to 400 MHz at three different temperatures for the two complexes (Fig. 8c). Relaxivity values decrease with increasing temperatures, which is characteristic of small molecular complexes, for which the rotation is limiting relaxivity. Moreover, the values are constant over a wide range of concentrations (Fig. S20†) indicating the absence of aggregation phenomenon. The relaxivities of GdImPy and GdPyPy are 8.25 mM^{-1} s^{-1} and 7.97 mM^{-1} s^{-1}, respectively, at 60 MHz and 25 °C. These are slightly higher than that of GdPy (7.57 mM^{-1} s^{-1}), and consistent with bishydrated complexes. The relaxivity is determined by several key physicochemical parameters, including the number of water molecules directly coordinated to Gd^{3+}, their water exchange rate, and the rotational correlation times. To accurately assess each of these parameters, NMRD measurements are typically complemented with ^{17}O NMR spectroscopy. Variable-temperature ^{17}O T_2 measurements provide infor-

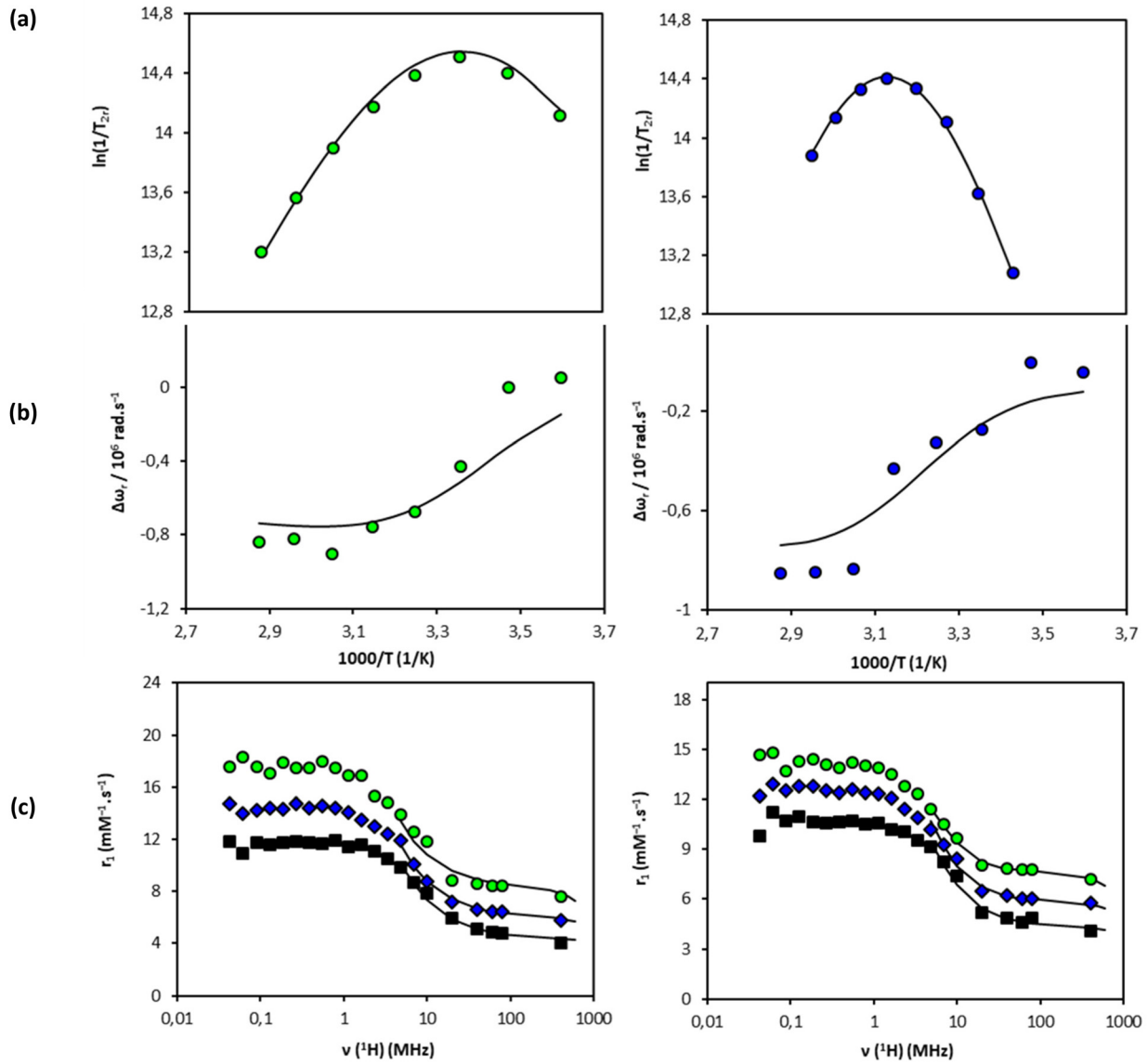

Fig. 8 Temperature dependence of the: (a) ^{17}O transverse relaxation rates, (b) chemical shifts at 9.4 T, and (c) NMRD profiles of GdImPy (left) and GdPyPy (right), respectively, at 25 °C (●), 37 °C (◆), and 50 °C (■). The curves represent the simultaneous fit to the experimental data points.

This journal is © The Royal Society of Chemistry 2025

Published on 26 February 2025. Downloaded on 4/3/2026 1:25:21 AM.

Table 6 Parameters obtained from the simultaneous fitting of the transverse ^{17}O relaxation rates and chemical shifts as a function of temperature at 9.4 T, and of the NMRD profiles at 25, 37, and 50 °C

	GdImPy	GdPyPy	GdHYD[15]	GdPTDITA[16]	GdPy[9]	GdDTPA[35]
k_{ex}^{298} (10^6 s^{-1})	9(2)	2.3(3)	7.8	3.3	9.3	3.3
$\Delta H^{\ddagger}$ (kJ mol^{-1})	44(6)	47(4)	43.5	37.7	50.4	51.6
τ_R^{298} (ps)	110(2)	104(3)	92.6	105	92[a]	58
E_R (kJ mol^{-1})	24(2)	22(2)	21.0	18	20.2	17.3
q	2	2	2	2	2	1
$A/\hbar$ (10^6 rad s^{-1})	−3.9(3)	−3.6(2)	−4.0	−3.3	−3.7	−3.8

mation about the water exchange rate (k_{ex}), while ^{17}O T_1 data offer insights into the rotational correlation time (τ_R). Additionally, ^{17}O chemical shifts indicate the number of water molecules directly coordinated to Gd^{3+} (q).

Longitudinal and transverse ^{17}O relaxation rates, along with chemical shifts, were measured as a function of temperature in aqueous solutions of GdImPy and GdPyPy, as well as in a diamagnetic reference ($HClO_4$, pH 3.3) at 9.4 T. The reduced ^{17}O longitudinal relaxation rates were too close to those of the reference and could not be used to determine the rotational correlation time. The reduced ^{17}O transverse relaxation rates and chemical shifts are presented in Fig. 8. The reduced chemical shifts are consistent with bishydrated complexes,[33] in accordance with luminescence lifetime measurements, and relaxivity values. Regarding the reduced ^{17}O transverse relaxation rates, it is clear from Fig. 8a that the behaviour of GdImPy and GdPyPy is quite different. The reduced relaxation rates increased with decreasing temperature up to 25 °C for GdImPy, whereas it increases up to 44 °C for GdPyPy. This means that the fast exchange region is more extended in terms of temperature for GdImPy compared to GdPyPy, leading to a faster exchange rate in the case of GdImPy. Nevertheless, for both complexes, the slow exchange region, where the reduced transverse relaxation rates decreased with decreasing temperatures, is well defined. In this region, $1/T_{2r}$ is directly determined by k_{ex}, allowing for its accurate determination.

The ^{17}O relaxation rates, chemical shifts, and NMRD profiles were analyzed using the Solomon–Bloembergen and Morgan (SBM) theory, which provided microscopic parameters characterizing water exchange and molecular rotation. The SBM approach is particularly useful for analyzing NMRD data at medium and high magnetic fields when detailed information about electron spin relaxation is not required,[34] and it offers reliable insights into dynamic processes like water exchange and rotational correlation times for small complexes. For this reason, only r_1 data above 4.83 MHz were included in the fitting process.

Several parameters were fixed to common values in the fitting of the data. The number of water molecules directly coordinated to Gd^{3+} (q) was fixed to 2. The Gd–O distance was fixed to an average value obtained by DFT calculations (2.56 Å) and we checked that variations from 2.55 Å to 2.61 Å did not vary significantly the results. The diffusion coefficient (D_t) was fixed to $2.6.10^{-9}$ m^2 s^{-1}, the Gd–water proton distance was fixed to 3.1 Å, while that of closest approach between Gd^{3+} and outer sphere protons to 3.6 Å.

Fig. 8c show the experimental value and the best fit, whose parameters are reported in Table 6 and S3.† The data could be fitted with a single k_{ex} value for both complexes with values of 9 × 10^6 for GdImPy and 2.3 × 10^6 s^{-1} for GdPyPy. Compared to GdPy (k_{ex} = 9.3 × 10^6 s^{-1}), the exchange rate is decreased in GdPyPy, consistent with the overall charge of the complex (the exchange rate increases with the negative charge of the complex).[3] However, for similar complex charges, k_{ex} of GdImPy is three times faster than that of GdPyPy. This could be related to the steric hindrance around the Gd^{3+} ion, as shorter $Ln–N_{im}$ distances have been found compared to those of $Ln–N_{Py'}$. Moreover, the presence of the close proton in the imidazole ring, could also participate to an overall faster exchange by H-bonding. Overall, the exchange rate of GdImPy is similar to that of GdPy despite the charge difference. The rotational correlation times (τ_R) are similar for GdImPy and GdPyPy, slightly higher than that of GdPy, and similar to that of GdPTDITA, which correlates well with the size of the complexes.

Finally, the r_1 values of GdImPy were measured as a function of pH and match very well with the distribution diagram (Fig. 9). The relativity values are constant in the pH range 4–8 and drop at pH > 8, indicating the formation of soluble hydroxocomplexes (GdLOH). At pH < 4, the r_1 starts to increase concurrently with the formation of the protonated (GdLH) species.

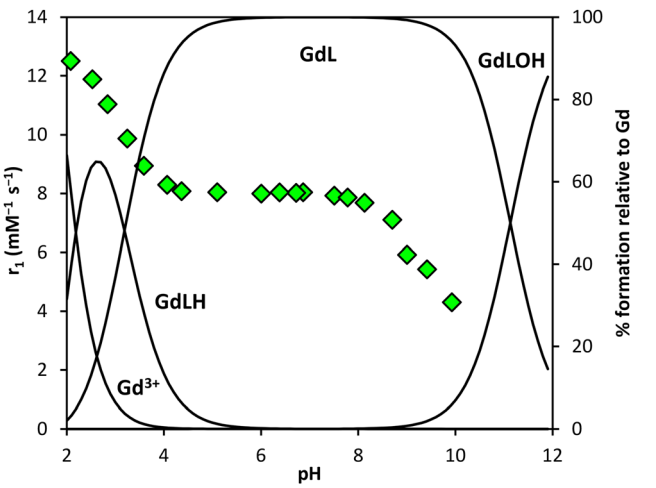

Fig. 9 pH-dependency of the ^1H relaxivity (60 MHz, 25 °C; ◆) of GdImPy (0.78 mM) along with the speciation diagram of a GdImPy system in a 1/1 ratio with the stability constants from Table 2.

Published on 26 February 2025. Downloaded on 4/3/2026 1:25:21 AM.

Anion interaction

For bishydrated complexes, maintaining high r_1 in biological environments depends on preventing the formation of ternary complexes. Indeed, endogenous anions like phosphate, carbonate, or citrate can displace those water molecules,[36–38] leading to a dramatic decrease in the relaxivity. Such phenomenon was not observed with negatively-charged GdPy,[8] but interestingly it was observed with GdPTDITA, suggesting that not only the charge was important but also probably the relative position of the two water molecules. We studied the r_1 of GdImPy and GdPyPy at pH 7.4 (HEPES buffer) and 25 °C while incrementally increasing concentrations of carbonate, phosphate, or citrate up to 50 equivalents (approximately 50 mM), as shown in Fig. 10. These levels far exceed the physiological concentrations found in human plasma, which are roughly 25 mM for carbonate, 1.1 mM for phosphate, and 0.11 mM for citrate.[39]

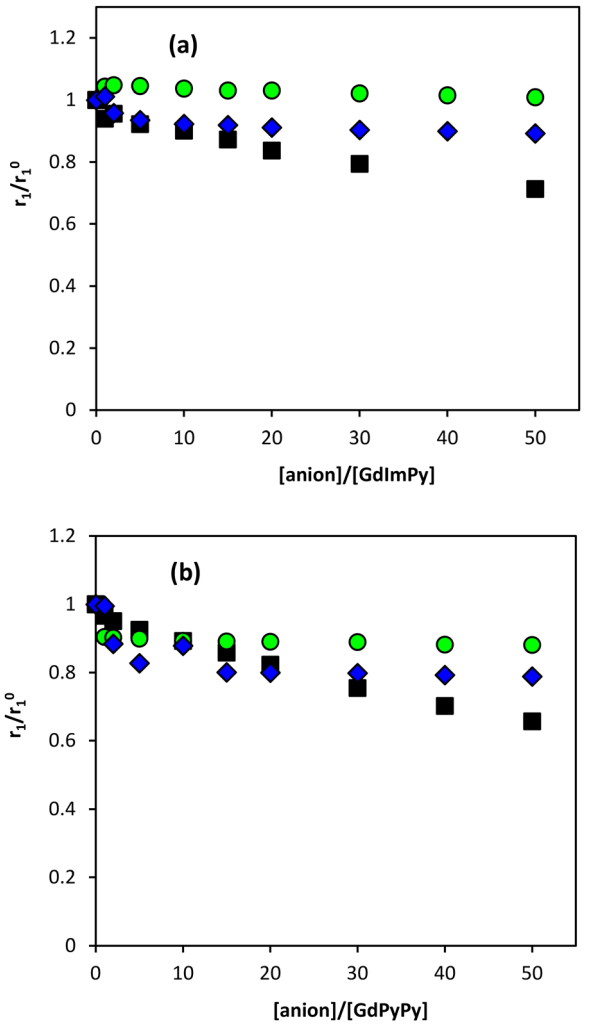

Fig. 10 Relaxivities measured (25 °C, pH = 7.4 in HEPES buffer 0.1 M at 60 MHz) in the presence of (a) GdImPy (1.28 mM) and (b) GdPyPy (1.80 mM), normalized to the initial value as a function of the concentration of citrate (●), phosphate (◆), and carbonate (■).

The addition of 5 equivalents of phosphate resulted in a small decrease of the relaxivity (7% GdPyPy and 17% GdImPy), similarly to what has been observed for GdHYD.[15] In this latter case, this was attributed to the presence of phosphate ions interacting with the ligand through hydrogen bonding, leading to an increased Gd–H_2O distance by reducing the number of second sphere water molecules. Here, to explore whether this reduction, especially in GdPyPy, was due to partial displacement of water molecules, we measured Eu^{3+} luminescence lifetimes in the presence and absence of 10 equivalents of phosphate (Table 7).

The number of coordinated water molecules remained close to 2 in both GdImPy and GdPyPy suggesting that the phosphate anions, which interact in a monodentate manner,[36] do not displace the inner-sphere water molecules.

Citrate anions can form bidentate interactions with bishydrated complexes.[36] Here, the relaxivity of GdImPy remains constant after the addition of 50 equivalents of citrate while that of GdPyPy is decreased by *ca.* 20%, indicating little to no formation of ternary complexes with citrate anions. This finding was supported by luminescence lifetime measurements of EuImPy and EuPyPy in the presence of 10 equivalents of citrate (Table 7) which shows q values very close to 2. However, in the case of small carbonate anions, which can also form bidentate interactions, the relaxivity of GdImPy and GdPyPy is decreased by 30 and 35%, respectively upon the addition of 50 eq. This is accompanied with a reduction in the number of water molecules to 1.3 and 1.1 for GdImPy and GdPyPy, respectively. Interestingly, this is in the same order of

Table 7 Eu^{3+} luminescence lifetimes (τ) for EuImPy and EuPyPy complexes (0.9 mM in 0.1 M HEPES buffer, pH/pD = 7) in the absence and presence of 10 equivalents of phosphate, carbonate, or citrate, and 50 equivalents of carbonate, along with the corresponding calculated q-values

	EuImPy	+10 eq. phosphate	+10 eq. carbonate	+10 eq. citrate	+50 eq. carbonate
τ_{H_2O} (ms)	0.390(5)	0.408(2)	0.406(3)	0.416(1)	0.516(2)
τ_{D_2O} (ms)	2.24(1)	2.15(1)	2.19(1)	2.12(1)	2.10(1)
q^a	2.0(2)	1.9(2)	1.9(2)	1.8(2)	1.3(2)
	EuPyPy	+10 eq. phosphate	+10 eq. carbonate	+10 eq. citrate	+50 eq. carbonate
τ_{H_2O} (ms)	0.406(8)	0.407(3)	0.404(2)	0.405(4)	0.547(3)
τ_{D_2O} (ms)	2.06(1)	2.03(1)	2.04(1)	1.95(1)	1.89(1)
q^a	1.9(2)	1.8(2)	1.9(2)	1.8(2)	1.1(2)

[a] Obtained from the empirical formula: $q = 1.11(\tau_{H_2O}^{-1} - \tau_{D_2O}^{-1} - 0.31)$.[31]

This journal is © The Royal Society of Chemistry 2025

Published on 26 February 2025. Downloaded on 4/3/2026 1:25:21 AM.

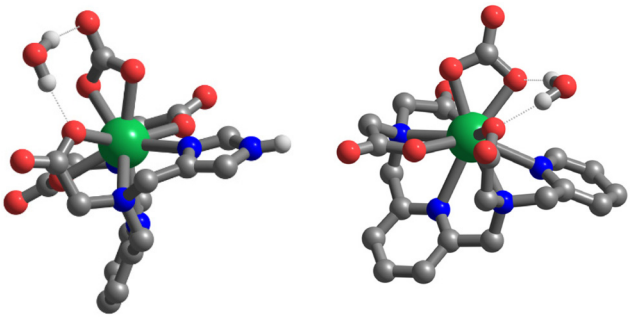

Fig. 11 Minimum energy structures of bidentate coordination of carbonate anion on (left) EuImPy or (right) EuPyPy.

magnitude as what has been observed for the negatively charged GdPTDITA for both carbonate and citrate interactions. This definitely indicates that the charge of the complex is not the only important factor. The differences observed between GdImPy and GdPyPy, as well as between carbonate and citrate for a given complex, suggest that the steric crowding around the Ln^{3+} ion also plays a role.

DFT calculations were performed on the Eu^{3+} complexes to determine the structure of the ternary complexes with carbonate. Optimisations were performed in continuum water and with one explicit water molecule. This water molecule could either be coordinated to Eu^{3+} with a carbonate bound in a monodentate mode, or be hydrogen bonded to the complex if the carbonate is bound in a bidentate manner (Fig. 11 and S21†). The results clearly show that the bidentate mode result in the lower energy structures with *ca.* 6.5 kcal mol^{-1} difference.

Altogether, this shows that the interaction of bishydrated complexes with physiological anions is quite complex, and the charge, steric crowding, and position of the water molecules play an intricate role in these interactions, with all these parameters being influenced by slight ligand modifications.

Conclusions

We have synthesized two new ligands, and characterized four Ln^{3+} complexes bearing one or two pendant imidazole or pyridine rings. The thermodynamic stability constants of the Ln^{3+}, Ca^{2+} and Zn^{2+} complexes were assessed by pH-potentiometric measurements. They show that the replacement of one carboxylate pendant arm by an imidazole or a pyridine does not have a strong effect on the stability constant of the corresponding complexes, while the replacement of two carboxylate functions is detrimental to the stability. From a kinetics perspective, we demonstrate that the dissociation processes occur mainly through acid-catalysed dissociation, similar to what was observed for the parent compound. The kinetic inertness is lower than that of GdPy, which could be related to the less constrained environment around the metal ion in EuPyPy or EuImPy, compared to EuPy (shorter Eu–O_{COO} distance compared to Eu–$N_{Im/Py}$). In the case of GdImPy, the presence of a labile protonated LnPyImH complex, also evidenced by NMR experiments, certainly plays a role. The kinetic inertness, in particular of GdPyPy, remains good considering the bishydrated character of the complexes.

From a structural point-of view, NMR experiments, luminescence lifetime measurements and DFT calculations indicate the coordination of the imidazole and the pyridine pendant rings in LnImPy or LnPyPy, leading to bishydrated complexes. The relaxivity values of the complexes GdImPy and GdPyPy are consistent with these findings. ^{17}O and NMRD data were fitted together and demonstrate a significant impact of replacing a carboxylate by a pyridine or an imidazole group on the water exchange rate. Interestingly for similarly charged complexes, the presence of the imidazole ring significantly accelerates the exchange rate compared to the pyridine arm. This could be related to the more crowded environment around the Ln^{3+} in the case of the imidazole. Interestingly, the presence of physiological anions do not strongly affect the relaxivity despite the neutral charge of the complexes. A relaxivity decrease of *ca.* 30% is observed with the addition of 50 eq. of carbonate, which could be related to a weak interaction of the anion with the complexes in a bidentate manner. The comparison with other complexes of this series evidence that the charge of the complex is not the only driving force for ternary complex formation, but the relative position of the water molecule is also important, as well as the steric crowding around the Ln^{3+} complex.

All together, this fundamental study gives new insight into the replacement of carboxylate functions by neutral aromatic rings bearing nitrogen atoms. This highlights that small modification on the ligand can slightly impact the structure of the corresponding complexes, but strongly impact their properties, such as the water exchange rate, the kinetic inertness, or the interaction with physiological anions.

Experimental part

Synthesis

See ESI.†

Liquid sample preparation

The concentrations of the stock solutions were determined by complexometric titration using a standardized Na_2H_2EDTA solution and appropriate indicators (eriochrome blackT ($CaCl_2$), xylenol orange ($ZnCl_2$ and $LnCl_3$), and murexide ($CuCl_2$)). Complexes were prepared by mixing 1 equivalent of ligand (L) with 1 equivalent of Ln^{3+}, and the pH was adjusted to 7.4 using a buffered solution or by adding NaOH or HCl. The absence of free Ln^{3+} ions were verified using the xylenol orange test. Additionally, the concentrations of the Ln^{3+}-containing solutions were verified by inductively coupled plasma optical emission spectrometry (ICP-OES) and, when feasible, bulk magnetic susceptibility (BMS) shift measurements.

Published on 26 February 2025. Downloaded on 4/3/2026 1:25:21 AM.

Potentiometric studies

Carbonate-free 0.1 M NaOH and 0.1 M HCl solutions were prepared from Fisher Chemicals concentrates. Potentiometric titrations were conducted in 0.1 M aqueous NaCl under an inert gas atmosphere (N_2) to avoid the presence of CO_2, with the temperature maintained at 25.0 ± 0.1 °C using a circulating water bath. p[H] (p[H] = −log[H^+], concentration in molarity) was measured with a combined pH glass electrode (Metrohm) filled with 3 M KCl, and titrant addition was automated using a 702 SM Titrino system (Metrohm). The electrode was calibrated by titrating HCl with NaOH in a 0.1 M electrolyte solution.[40] A plot of meter reading *versus* p[H] was used to determine the electrode standard potential ($E°$) and slope factor (f). Continuous potentiometric titrations with 0.1 M HCl and 0.1 M NaOH were performed on aqueous solutions containing 5 mL of ligand (L) in 0.1 M NaCl, with a 2 minute interval between successive points. The titrations of the metal complexes were performed with the same ligand solutions containing 1 or 2 equiv. of metal cation, with 2 min waiting time between two points. Experimental data were refined using Hyperquad 2008 software.[41] All equilibrium constants are reported as concentration quotients rather than activities and are defined as:

$$K_{mhl} = \frac{[M_m L_l H_h]}{[M]^m [L]^l [H]^h} \quad (11)$$

At 25 °C and an ionic strength of 0.1 mol L^{-1}, the ionic product of water is pK_w = 13.77.[42] Fixed values were used for pK_w, as well as for the acidity constants of the ligands and the total concentrations of metal, ligand, and acid. All reported values and errors (one standard deviation) are the averages from at least three independent experiments.

UV-Visible measurements

UV-visible absorption spectra were recorded at 25 °C on a PerkinElmer UV/Vis/NIR Lambda 19 spectrometer in the range λ = 200–900 nm with data steps of 1 nm, with a 1 cm path length.

For the stability constant of the CuImPy, CuIm2Py and CuPyPy complexes, out-of-cell (batch) samples were prepared containing the ligand (2.5 mM) and Cu^{2+} (2.5 mM) by applying slight ligand excess. The samples' ranged from pH 0 to 2, and they were equilibrated for one day. The measurements were performed at 25 °C, using thermostated semimicro 3 mm cells.

Luminescence and lifetime measurements

Measurements were performed on an Agilent Cary Eclipse fluorescence spectrophotometer. Emission spectra were recorded using the following excitation wavelengths and concentrations: [EuImPy] = 67 μM (λ_{exc} = 262 nm), [EuIm2Py] = 116 μM (λ_{exc} = 263 nm), [EuPyPy] = 95 μM, (λ_{exc} = 261 nm), [EuPy3] = 93 μM (λ_{exc} = 262 nm), and [EuPy] = 89 μM, (λ_{exc} = 262 nm). All samples were prepared in 0.1 M HEPES buffer at pH 7.4.

Luminescence lifetimes were determined by measuring the decay of emission intensity at 616 nm in H_2O and D_2O solutions in HEPES buffer 0.1M at pH/pD 7. For the anion interaction, ten equivalents of citrate/phosphate/carbonate were added to both solutions, and also 50 equivalents of carbonate. The settings were as follow: gate time, 0.1 ms; delay time, 0.1 ms; flash count, 1; total decay time, 10 ms; 100 cycles; PMT detector, 800 mV. At least three decay curves were collected for each sample, all lifetimes were analyzed as mono exponential decays. The reported lifetimes are an average of at least three measurements.

NMR spectroscopy

^{1}H and 2D ^{1}H/^{1}H or ^{1}H/^{13}C (COSY, HSQC and HMBC) NMR spectra were recorded on a Bruker Avance III HD Spectrometer using a 5 mm BBFO probe. ^{1}H and ^{13}C were obtained respectively at 600 MHz and 150 MHz. The spectra were recorded in D_2O at 25 °C, otherwise stated. When necessary, a solvent suppression was performed using an excitation sculpting sequence. pH titrations of ImPy (7.01 mM), YImPy (7.1 mM), and YPyPy (7.2 mM) were performed with NaOD 1 M (pD = pH_{read} + 0.41).[43] The protonation constant were fitted using HypNMR.[20]

EPR spectroscopy

Samples of CuImPy (1.08 mM) and CuPyPy (1.10 mM) were transferred into 3 mm internal diameter quartz capillaries (Wilmad-LabGlass, New Jersey, USA). 20% (v/v) of glycerol was added before flash freeze in liquid nitrogen. Continuous wave EPR spectra were recorded at a temperature of 30 K with a Bruker EMX plus spectrometer (Bruker Biospin, Rheinstetten, Germany) equipped with an ESR-900 Helium flow cryostat (Oxford Instruments, Oxfordshire, UK) and an ER 4122SHQE Bruker cavity operating at 9.39 GHz. Microware power was set to 23 μW and modulation amplitude to 5 G.

Temperature-dependent ^{17}O NMR measurements

The transverse ^{17}O relaxation rates ($1/T_2$, $1/T_1$) and chemical shifts were measured in aqueous solutions of GdImPy and GdPyPy (9.14 mM and 7.15 mM, pH 7.4 HEPES buffer) over a temperature range of 5–75 °C using a Bruker Avance 400 spectrometer (9.4 T, 54.5 MHz). Temperature calibration was performed based on prior calibrations with ethylene glycol and methanol.[44] An acidified water solution ($HClO_4$, pH 3.3) served as the external reference. Longitudinal relaxation times (T_1) were determined using the inversion-recovery method, while transverse relaxation times (T_2) were obtained *via* the Carr–Purcell–Meiboom–Gill spin-echo technique.[45] The methodology for ^{17}O NMR measurements on Gd^{3+} complexes has been previously described.[46] Samples were sealed in glass spheres fitted into 10 mm NMR tubes to avoid susceptibility corrections of the chemical shifts.[47] To enhance sensitivity, ^{17}O-enriched water (10% $H_2{}^{17}O$) was added to the solutions to achieve approximately 1% enrichment. The ^{17}O NMR data were analyzed according to the Solomon–Bloembergen–Morgan theory of paramagnetic relaxation (see ESI†). The

 This journal is © The Royal Society of Chemistry 2025

Published on 26 February 2025. Downloaded on 4/3/2026 1:25:21 AM.

least-squares fitting of the ^{17}O NMR data was performed using Visualiseur/Optimiseur software[48] running on a MATLAB 8.3.0 (R2014a) platform.

Relaxometric measurements

Proton relaxation rate ($1/T_1$) measurements as a function of pH, concentration or in the presence of anions were performed at 25 °C and 60 MHz on the minispec Brucker "mqvar" relaxometer. The temperature was monitored by a Julabo CD-200F temperature control unit. T_1 were measured with an inversion recovery sequence, and at least 3 reproducible measurements were performed. The experimental errors are ±5%. The Gd^{3+} concentration of the sample was controlled by ICP (Inductively Coupled Plasma).

For GdImPy, measurements were performed at 0.78 mM as a function of pH in the range of 2.1–9.9.

To determine the longitudinal relaxivity (r_1) values, different concentrations of GdImPy (0–9 mM) and GdPyPy (0–7 mM) were prepared. Linear fitting of the reciprocal of the paramagnetic relaxation rates (R_1) *vs.* the Gd concentration (mM) was used to estimate r_1 ($mM^{-1}\ s^{-1}$).

The influence of the anion was measured for GdImPy (1.28 mM) and GdPyPy (1.80 mM) in HEPES buffer 0.1 M, pH = 7.4 at 25 °C with varying additions of citrate, carbonate, and phosphate.

NMRD profiles: Measurements were recorded at 2.28 mM for GdImPy and 2.23 mM for GdPyPy in HEPES buffer (0.1 M, pH 7.4) on a Stelar SMARTracer fast field cycling relaxometer (0.01–10 MHz) and a Bruker WP80 NMR electromagnet adapted to variable field measurements (20–80 MHz) and controlled by a SMARTracer PC-NMR console. The temperature was monitored by a VTC91 temperature control unit and maintained by a gas flow. The temperature was determined by previous calibration with a Pt resistance temperature probe. The least-squares fit of the ^1H NMRD data and simultaneous fit with the ^{17}O NMR data were analyzed according to the Solomon–Bloembergen–Morgan theory of paramagnetic relaxation (see ESI†). The least-squares fitting of the data was performed using Visualizeur/Optimiseur[48] running on a MATLAB 8.3.0 (R2014a) platform.

Dissociation kinetic studies

The kinetic inertness of GdImPy and GdPyPy was assessed at 25 °C and in 0.1 M NaCl *via* transmetallation studies of GdImPy (126 μM) and GdPyPy (122 μM) with Eu^{3+} (10-fold excess) at pH 4.7–5.45 and pH 3.7–5.05, respectively (0.02 M dimethylpiperazine below pH 4.7 and *N*-methylpiperazine above). The excess of the exchanging metal ion guarantees the pseudo-first order conditions. The pH was controlled for each sample at the end of the kinetic measurements to confirm that it remained stable during the experiment. In all cases, the reactions were monitored by measuring the Eu^{3+} emission on an Agilent Cary Eclipse Fluorescence spectrophotometer. The experimental errors are ±5%. The analysis of the experimental data was performed using Visualiseur/Optimiseur[48] running on a MATLAB 8.3.0 (R2014a) platform.

DFT calculations

The structures of the complexes were obtained by DFT calculations employing the ωB97xD functional[49] and the 6-31+G(d) basis set for all atoms of the ligands and the MWB52 Stuttgart-Dresden quasi-relativistic pseudopotential and the associated basis set for valence electrons for the Eu.[50] Solvent effect was included by employing the polarizable continuum model (PCM).[51] All calculations were run with Gaussian16 rev. A.03.[52]

Author contributions

MS: investigation and vizualisation, writing – original draft. LC: investigation and vizualisation. HM: investigation and vizualisation. JFM: investigation and supervision. ZG: investigation. AP: investigation and vizualisation, supervision. SG: investigation and vizualisation. AM: investigation, writing – original draft. C.S.B: conceptualization, project management, supervision, funding acquisition, writing – original draft.

Data availability

The data supporting this article have been included as part of the ESI.†

Conflicts of interest

There are no conflicts to declare.

Acknowledgements

The authors acknowledge the support from the MITI CNRS Metallomix, La Ligue Contre le Cancer (comités du Loir et Cher, du Loiret, du Morbihan), and la Maison de la Chimie. Financial support from the IR INFRANALYTICS FR2054 for conduction of this research is gratefully acknowledged. We also thank the SALSA and MO2VING platforms for spectroscopic measurements (NMR, MS, HRMS).

References

1 J.-C. G. Bünzli, *Coord. Chem. Rev.*, 2015, **293–294**, 19–47.
2 L. A. Marchetti, M. Isaac and C. S. Bonnet, in *Lanthanide and Other Transition Metal Ion Complexes and Nanoparticles in Magnetic Resonance Imaging*, CRC Press, 2024.
3 A. Merbach, L. Helm and E. Toth, *The Chemistry of Contrast Agents in Medical Magnetic Resonance Imaging*, John Wiley & Sons, Ltd, 2013.
4 J. Wahsner, E. M. Gale, A. Rodríguez-Rodríguez and P. Caravan, *Chem. Rev.*, 2019, **119**, 957–1057.
5 R. Uzal-Varela, A. Rodríguez-Rodríguez, H. Wang, D. Esteban-Gómez, I. Brandariz, E. M. Gale, P. Caravan and C. Platas-Iglesias, *Coord. Chem. Rev.*, 2022, **467**, 214606.

Published on 26 February 2025. Downloaded on 4/3/2026 1:25:21 AM.

6 P. Caravan, D. Esteban-Gómez, A. Rodríguez-Rodríguez and C. Platas-Iglesias, *Dalton Trans.*, 2019, **48**, 11161–11180.
7 L. A. Loevner, B. Kolumban, G. Hutóczki, K. Dziadziuszko, D. Bereczki, A. Bago and A. Pichiecchio, *Invest. Radiol.*, 2023, **58**, 307.
8 L. Pellegatti, J. Zhang, B. Drahos, S. Villette, F. Suzenet, G. Guillaumet, S. Petoud and É. Tóth, *ChemComm*, 2008, 6591–6593.
9 C. S. Bonnet, F. Buron, F. Caillé, C. M. Shade, B. Drahoš, L. Pellegatti, J. Zhang, S. Villette, L. Helm, C. Pichon, F. Suzenet, S. Petoud and É. Tóth, *Chem. – Eur. J.*, 2012, **18**, 1419–1431.
10 F. Caillé, C. S. Bonnet, F. Buron, S. Villette, L. Helm, S. Petoud, F. Suzenet and É. Tóth, *Inorg. Chem.*, 2012, **51**, 2522–2532.
11 C. S. Bonnet, F. Caillé, A. Pallier, J.-F. Morfin, S. Petoud, F. Suzenet and É. Tóth, *Chem. – Eur. J.*, 2014, **20**, 10959–10969.
12 K. P. Malikidogo, M. Isaac, A. Uguen, S. Même, A. Pallier, R. Clémençon, J.-F. Morfin, S. Lacerda, É. Tóth and C. S. Bonnet, *Chem. Commun.*, 2023, **59**, 12883–12886.
13 K. P. Malikidogo, M. Isaac, A. Uguen, J.-F. Morfin, G. Tircsó, É. Tóth and C. S. Bonnet, *Inorg. Chem.*, 2023, **62**, 17207–17218.
14 H. Martin, A. Uguen, J.-F. Morfin, M. Isaac, A. Pallier, A. Melchior and C. Bonnet, *Chem. – Eur. J.*, 2024, e202403861.
15 C. S. Bonnet, S. Laine, F. Buron, G. Tircsó, A. Pallier, L. Helm, F. Suzenet and É. Tóth, *Inorg. Chem.*, 2015, **54**, 5991–6003.
16 Z. Baranyai, L. Tei, G. B. Giovenzana, F. K. Kálmán and M. Botta, *Inorg. Chem.*, 2012, **51**, 2597–2607.
17 S. Laine, R. Jouclas, C. S. Bonnet, P. Retailleau, V. Steinmetz, A. Pallier, Z. Garda, G. Tircsó, P. Durand and É. Tóth, *Eur. J. Inorg. Chem.*, 2024, **27**, e202300784.
18 E. Caillet, L. Nunes, S. V. Eliseeva, M. Ndiaye, M. Isaac, A. Pallier, J.-F. Morfin, H. Meudal, S. Petoud, S. Routier, C. Platas-Iglesias, F. Buron and C. S. Bonnet, *Dalton Trans.*, 2024, **53**, 9028–9041.
19 M. Sanadar, L. Collobert, J.-F. Morfin, J.-M. Mouesca, S. Gambarelli and C. S. Bonnet, *In preparation*.
20 C. Frassineti, L. Alderighi, P. Gans, A. Sabatini, A. Vacca and S. Ghelli, *Anal. Bioanal. Chem.*, 2003, **376**, 1041–1052.
21 H. Sigel, P. R. Huber and R. Griesser, *Inorg. Chem.*, 1971, **10**, 945–947.
22 T. W. Duma, F. Marsicano and R. D. Hancock, *J. Coord. Chem.*, 1991, **23**, 221–232.
23 M. Regueiro-Figueroa, E. Ruscsák, L. Fra, G. Tircsó, I. Tóth, A. de Blas, T. Rodríguez-Blas, C. Platas-Iglesias and D. Esteban-Gómez, *Eur. J. Inorg. Chem.*, 2014, 6165–6173.
24 A. Rodríguez-Rodríguez, Z. Garda, E. Ruscsák, D. Esteban-Gómez, A. de Blas, T. Rodríguez-Blas, L. M. P. Lima, M. Beyler, R. Tripier, G. Tircsó and C. Platas-Iglesias, *Dalton Trans.*, 2015, **44**, 5017–5031.
25 L. Sarka, L. Burai and E. Brücher, *Chem. – Eur. J.*, 2000, **6**, 719–724.
26 S. Mizzoni, S. Ruggieri, A. Sickinger, F. Riobé, L. Guy, M. Roux, G. Micouin, A. Banyasz, O. Maury, B. Baguenard, A. Bensalah-Ledoux, S. Guy, A. Grichine, X.-N. Nguyen, A. Cimarelli, M. Sanadar, A. Melchior and F. Piccinelli, *J. Mater. Chem. C*, 2023, **11**, 4188–4202.
27 S. Mizzoni, A. Sickinger, S. Ruggieri, F. Riobé, L. Guy, O. Maury, B. Baguenard, A. Bensalah-Ledoux, Y. Guyot, S. Guy, M. Sanadar, A. Melchior and F. Piccinelli, *New J. Chem.*, 2024, **48**, 9627–9636.
28 S. Ruggieri, S. Mizzoni, C. Nardon, E. Cavalli, C. Sissa, M. Anselmi, P. G. Cozzi, A. Gualandi, M. Sanadar, A. Melchior, F. Zinna, O. G. Willis, L. Di Bari and F. Piccinelli, *Inorg. Chem.*, 2023, **62**, 8812–8822.
29 A. N. Carneiro Neto, R. T. J. Moura, L. D. Carlos, O. L. Malta, M. Sanadar, A. Melchior, E. Kraka, S. Ruggieri, M. Bettinelli and F. Piccinelli, *Inorg. Chem.*, 2022, **61**, 16333–16346.
30 C. De Rosa, A. Melchior, M. Sanadar, M. Tolazzi, A. Giorgetti, R. P. Ribeiro, C. Nardon and F. Piccinelli, *Inorg. Chem.*, 2020, **59**, 12564–12577.
31 R. M. Supkowski and W. D. W. Horrocks, *Inorg. Chim. Acta*, 2002, **340**, 44–48.
32 F. Benetollo, G. Bombieri, S. Aime and M. Botta, *Acta Crystallogr., Sect. C:Cryst. Struct. Commun.*, 1999, **55**, 353–356.
33 É. Tóth, L. Helm and A. Merbach, in *The Chemistry of Contrast Agents in Medical Magnetic Resonance Imaging*, John Wiley & Sons, Ltd, 2013, pp. 25–81.
34 P. H. Fries and E. Belorizky, in *The Chemistry of Contrast Agents in Medical Magnetic Resonance Imaging*, John Wiley & Sons, Ltd, 2013, pp. 277–309.
35 D. H. Powell, O. M. N. Dhubhghaill, D. Pubanz, L. Helm, Y. S. Lebedev, W. Schlaepfer and A. E. Merbach, *J. Am. Chem. Soc.*, 1996, **118**, 9333–9346.
36 M. Botta, S. Aime, A. Barge, G. Bobba, R. S. Dickins, D. Parker and E. Terreno, *Chemistry*, 2003, **9**, 2102–2109.
37 C. De Rosa, A. Melchior, M. Sanadar, M. Tolazzi, A. Duerkop and F. Piccinelli, *Dalton Trans.*, 2021, **50**, 4700–4712.
38 S. R. Kiraev, R. R. Weber, J. A. L. Wells, A. Orthaber, D. Kovacs and K. E. Borbas, *Analysis Sensing*, 2022, **2**, e202200015.
39 G. J. Tortora and N. P. Anagnostakos, *Principles of anatomy and physiology*, Harper & Row, New York, NY, 6th edn, 1990.
40 A. E. Martell and R. J. Motekaitis, *Determination and Use of Stability Constants*, Wiley-VCH, 1992.
41 P. Gans, A. Sabatini and A. Vacca, *Talanta*, 1996, **43**, 1739–1753.
42 R. M. Smith, R. J. Motekaitis and A. E. Martell, *National Institute of Standards and Technology*, NIST Standard Reference Database, 1997.
43 P. K. Glasoe and F. A. Long, *J. Phys. Chem.*, 1960, **64**, 188–190.
44 D. S. Raiford, C. L. Fisk and E. D. Becker, *Anal. Chem.*, 1979, **51**, 2050–2051.
45 S. Meiboom and D. Gill, *Rev. Sci. Instrum.*, 1958, **29**, 688–691.

 This journal is © The Royal Society of Chemistry 2025

Published on 26 February 2025. Downloaded on 4/3/2026 1:25:21 AM.

46 K. Micskei, L. Helm, E. Brucher and A. E. Merbach, *Inorg. Chem.*, 1993, **32**, 3844–3850.
47 A. D. Hugi, L. Helm and A. E. Merbach, *Helv. Chim. Acta*, 1985, **68**, 508–521.
48 F. Yerly, *Visualiseur 2.3.5 and Optimiseur 2.3.5*, Lausanne, Switzerland, 1999.
49 J. D. Chai and M. Head-Gordon, *Phys. Chem. Chem. Phys.*, 2008, **10**, 6615–6620.
50 M. Dolg, H. Stoll and H. Preuss, *J. Chem. Phys.*, 1989, **90**, 1730–1734.
51 J. Tomasi, B. Mennucci and R. Cammi, *Chem. Rev.*, 2005, **105**, 2999–3093.
52 M. J. Frisch, G. W. Trucks, H. B. Schlegel, G. E. Scuseria, M. A. Robb, J. R. Cheeseman, G. Scalmani, V. Barone, G. A. Petersson, H. Nakatsuji, X. Li, M. Caricato, A. V. Marenich, J. Bloino, B. G. Janesko, R. Gomperts, B. Mennucci, H. P. Hratchian, J. V. Ortiz, A. F. Izmaylov, J. L. Sonnenberg, D. Williams-Young, F. Ding, F. Lipparini, F. Egidi, J. Goings, B. Peng, A. Petrone, T. Henderson, D. Ranasinghe, V. G. Zakrzewski, J. Gao, N. Rega, G. Zheng, W. Liang, M. Hada, M. Ehara, K. Toyota, R. Fukuda, J. Hasegawa, M. Ishida, T. Nakajima, Y. Honda, O. Kitao, H. Nakai, T. Vreven, K. Throssell, J. A. Montgomery Jr., J. E. Peralta, F. Ogliaro, M. J. Bearpark, J. J. Heyd, E. N. Brothers, K. N. Kudin, V. N. Staroverov, T. A. Keith, R. Kobayashi, J. Normand, K. Raghavachari, A. P. Rendell, J. C. Burant, S. S. Iyengar, J. Tomasi, M. Cossi, J. M. Millam, M. Klene, C. Adamo, R. Cammi, J. W. Ochterski, R. L. Martin, K. Morokuma, O. Farkas, J. B. Foresman and D. J. Fox, *Gaussian 16 Rev.A03*, Wallingford, CT.